

# A realistic nonlinear benchmark problem for wave energy controllers - COERbuoy1

Simon H. Thomas, Jørgen Hals Todalshaug, John V. Ringwood.

**Abstract**—This paper presents a realistic, nonlinear numerical open-source benchmark model for Wave Energy Converters (WECs) to facilitate the effective comparison of WEC control strategies. The model represents a point-absorber WEC, and was developed in cooperation with CorPower Ocean to obtain a realistic control problem (COERbuoy1), constituting real device characteristics. At the same time, the model is sufficiently representative of the broad class of point absorbers to allow universal findings.

The hydrodynamic forces are calculated using instantaneous linearisation of the hydrodynamic parameters for body-exact wave-body interactions in two degrees of freedom. Additionally, the model includes nonlinear effects such as viscous drag, static and dynamic friction, a power-take-off using an electric generator with saturation effects, and a nonlinear spring opposing the hydrostatic stiffness. The benchmark problem consists of three stages: Testing the control performance in (1) regular and (2) irregular waves and by (3) using small modifications in the model to challenge the controller's ability to handle modelling errors. The benchmark scoring system evaluates the controller on the basis of the absorbed power and adherence to motion and power constraints.

The system is tested with an illustrative constant damping power-take-off, showing reasonably good results in power absorption for low period cases, but poor results for long wave periods.

**Index Terms**—Wave energy, control, benchmarking, nonlinear model, body-exact

## I. INTRODUCTION

THE wave energy sector is characterised by a wide range of concepts as how best to generate electric energy from the energy transported in ocean waves. A good overview of such concepts is given in [1] and [2]. Considering all concepts, point-absorbers are one of the most promising [3], whereby a small (relative to the wavelength) buoy interacts with the wave, which then drives a generator.

Controlling a Point Absorber Wave Energy Converter (PAWEC) is fundamentally different from many other control tasks [4], since:

- Instead of aiming to stabilise a system about an equilibrium point, PAWEC controllers, to maximise the energy absorption, should maximise the use of the available stroke length, resulting in a highly nonlinear behaviour for common PAWEC shapes.

This work was funded by CorPower Ocean AB and Science Foundation Ireland. It was supported by MaREI."

S.T. Centre for Ocean Energy Research, National University of Ireland Maynooth, Maynooth, Ireland

J.H. CorPower Ocean AB, Västberga Alleé 60, 12630 Hägersten, Stockholm, Sweden

J.R. Centre for Ocean Energy Research, National University of Ireland Maynooth, Maynooth, Ireland

- While many controlled systems act under well known, constant, conditions, PAWECs operate in the ocean under varying wave conditions, depending on the location, the season and the local and global wave climate. Sea states may range from large to small waves, with narrow-band spectra to wide-band spectra.
- While aiming to maximise converted energy in varying conditions, the controller must ensure that the machine operates within its physical constraints.

A variety of control strategies, to increase the power production of WECs, exist [5], and are evaluated for a range of PAWEC designs. Due to the strong coupling between the ideal control and optimal WEC design, it can be a challenge to separate the effects/dynamics of the controller from the WEC [6], thus prohibiting a straightforward comparison of control strategies between reported studies, and so ultimately preventing the research community from evaluating different control concepts on a level playing field.

In the past, there have been several attempts to compare control strategies; some papers reviewed control strategies or even provided detailed comparisons between different controller types [5], [7]–[9]. Another approach is WECCComp [10], a competition for WEC controllers including numerical simulation and wave tank tests, where several control strategies competed against each other, for a standard WEC system consideration.

Control is inseparably connected with system-design [6], since the controller adapts the system to fulfil a specific target. Designing a controller, without targeting a specific system, may be as fruitless as designing a system without the control in mind. WEC controllers are influenced by all components in a system and, as such, requires WEC models designed for control evaluation to thoroughly model all relevant components, from the wave-buoy interactions to the electric energy conservation. Such models are termed Wave-to-Wire (W2W) models. Developing a realistic W2W model can be more demanding than the controller itself and, as a result, many controllers are tested against models focusing only on specific effects.

To give the control developers a realistic WEC model to evaluate their controller against, the COERbuoy1 model, with an integrated benchmarking tool, is developed, which aims to cover all significant effects of a real WEC device and is general enough to allow universal findings. The COERbuoy1 platform goes beyond the majority of existing W2W concepts [11] by:

- Calculating body-exact hydrodynamic forces.
- Simulating generator saturation.
- Being based on an existing, industrial WEC design.
- Offering a control interface, allowing hassle-free integration of prototype controllers.
- Proposing a scoring system to benchmark the controller, with a comprehensive range of test scenarios, featuring regular and irregular waves, systematic bias of the model description, and operational constraints.
- Being open-source.

To achieve a realistic model, COERbuoy1 was designed in close collaboration with the Swedish-based WEC company CorPower Ocean AB, who have a decade of experience with scaled and full-scale prototypes of their CorPower WEC design. Even though it is inspired, in some aspects, by the CorPower WEC, the COERbuoy1 model is an independent WEC design.

The remainder of this paper is organised as follows: In Section II, the characteristics of the COERbuoy1 model are described. Section III then gives a brief overview of the mathematical modelling approaches employed, before Section IV introduces the scoring system for the benchmark. As an example, an uncontrolled WEC, using a constant generator damping, is benchmarked in Section V. Finally, in Section VI, a brief technical outline of the model is presented and, in Section VII, conclusions are given.

## II. THE COERBUOY1 WEC MODEL

The COERbuoy1 (the naming convention refers to the Center for Ocean Energy Research's abbreviation COER and ensures the benchmark device can be distinguished from potential successors) device was derived from the experience of the CorPower team with real WECs, by first identifying the most significant features and then choosing a level of detail for their implementation. Subsection II-A will give a brief overview of this process. Following this, constraint handling is elucidated in Subsection II-B, then the three different operational characteristics a controller has to handle are presented in II-C. This section is concluded with an overview of the notionally installed sensors and available manipulated variables.

### A. Features

The CorPower device is a good example of a device designed with control in mind: Its natural frequency is, even in the absence of external control, close to typical wave frequencies. This behaviour is achieved by a spring opposing the buoyancy stiffness ('negative spring'), furthermore offering a reactive controllable electric generator and a mechanical friction brake, giving the control developer the freedom to use a wide variety of different control approaches. An important step in developing a controller is model reduction, to potentially simplify the device model and make it implementable and computationally affordable, particularly within a model-based control strategy. To this end, a decision matrix is used which was solved in collaboration with the CorPower team, to weight the

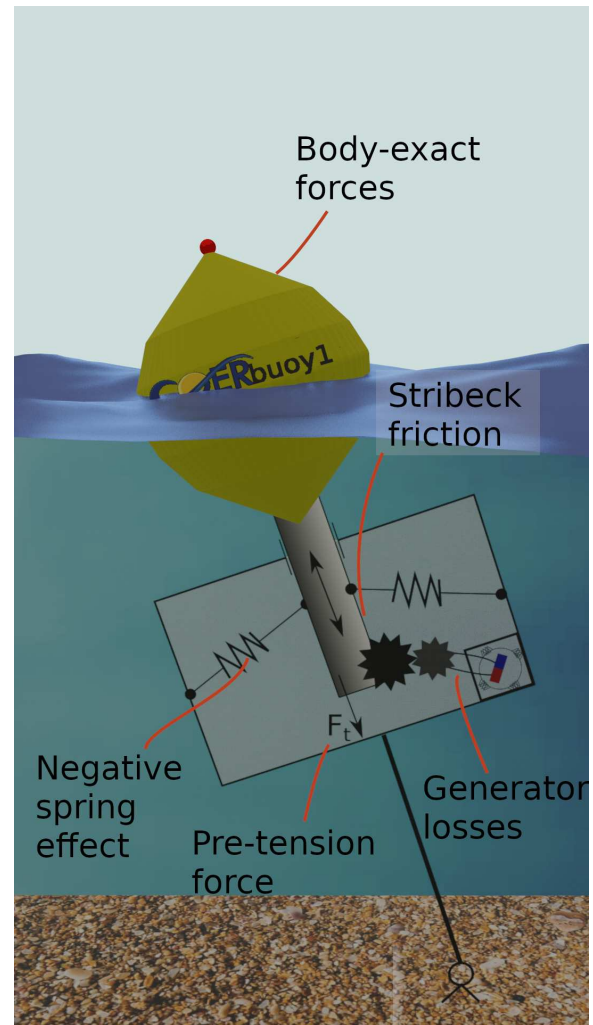


Fig. 1. Sketch of the COERbuoy1 WEC and the effects it simulates.

significance of all components and effects relevant to control and computational performance. While COERbuoy1 is, in many aspects, inspired by the CorPower device, it is an independent, generalized WEC concept, incorporating ideas from different WEC designs and therefore designed to facilitate universal findings. Here, a brief overview of the features included in the model is given, with the full decision matrix seen in Table I:

- **Degrees of freedom** From the experience of the CorPower team, the heave, followed by the surge component, are deemed to be the most important. Pitch is deemed to have a minor influence, by comparison. Roll, sway and yaw are rarely manifest with an ideal CorPower device. However, sway and pitch can play an important role in generating potential dynamic instability under certain conditions, but an accurate calculation is complex and computationally demanding. In summary, considering the forgoing rationale, heave and surge motion is implemented in the model, the DOF that primarily effect the PTO action, while pitch, roll, sway and yaw are neglected.
- **Shape** Many devices have a curved vertical profile, thus their hydrodynamic forces are highly dependent on the instantaneous submergence level

TABLE I  
DECISION MATRIX

Effects	Importance [I] (1-3)	Model representation	Accuracy [A] (1-5)	Computational costs [C] (1-10)	Sum I-A-C
<b>Buoy</b>					
Hydro. modelling	3	BEM, linearised at mean position	1	1	2
	3	Body-exact FK-force, but linear diffraction and radiation	2	3	3
	3	Body-exact forces using pre-calculated BEM data stored in a LUT	3	3	6
	3	CFD	5	10	5
Viscous drag	2	excluded	1	1	2
	2	included	3	2	7
<b>Machinery</b>					
friction	2	linear damping	2	1	5
	2	Coulomb	3	3	6
	2	Coulomb+damping (Stribeck)	4	4	8
generator	3	no losses	2	1	5
	3	efficiency factor	3	2	7
	3	cooper+iron losses + saturation	4	3	9
	3	... + transient behaviour	5	10	5
<b>Other</b>					
mooring	2	stiff	1	1	2
	2	spring-damper	2	8	-2
	2	lump-model	3	10	-1

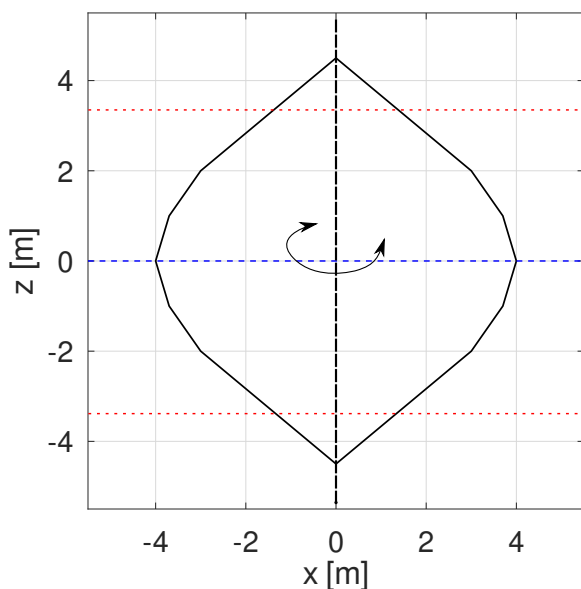


Fig. 2. Cross section of the COERbuoy1 shape: The blue dashed line indicates the water level at the device equilibrium position, the red dotted lines at  $z = \pm 3.5$  m are placed at the stroke limit (for the heave only case).

of the buoy. Linearisation of the hydrodynamic forces about the equilibrium position may lead to significant errors, when there is a large offset between the equilibrium point and the buoy position. As a result, hydrodynamic forces are based on a body-exact formulation.

- **Friction** is typically seen as one of the main forces acting on the system during low-energy sea states. While bearings and the generator gearing system introduce a velocity dependent friction force, for low energy sea states, the stick-slip effect has a major contribution to device behaviour. To capture these effects, a Stribeck based friction model is used, here modelled as a combination of Coulomb friction, including a static and a dynamic term, and

a velocity dependent friction.

- **Braking** For safety and maintenance operation, most WECs feature a mechanical friction brake. In the COERbuoy1 device, this brake can be controlled, with the braking force only limited by the maximum braking power limit.
- **Generator** Electrical generators are widely used in PAWECs [12] [13], which can be translational or rotational, where a gearbox transforms the translational movement into a rotational one. From a control perspective, both concepts behave similarly. The CorPower WEC uses a rotatory generator, which can additionally be used in motoring mode, putting power into the system, and therefore allowing bidirectional power flow. However, due to losses in the generator, only part of the absorbed energy is transformed into electrical energy and similarly for reactive power flow. Furthermore, the maximal power that can be absorbed or applied is limited by the motor characteristics. The unit is modelled as a permanent magnet generator/motor, using an R-L circuit and incorporating the effects of magnetic saturation. Transient effects are assumed to be several orders of magnitude faster than the WEC dynamics and are therefore neglected.
- **Moorings** Anchored on the seabed, a mooring connection provides a reactive force keeping the WEC in place, with different WEC designs using fibre ropes, stiff rods or chains. The CorPower mooring can be described as a stiff rod, subject to both tension and compression forces. Furthermore, it provides a pre-tension, allowing the WEC gravity force (and thus inertia) to be lower than the buoyancy force at equilibrium. While the mooring line is an essential part of the WEC, and its pre-tension has a significant effect on the WEC characteristics, the computational costs to calculate the mooring as a multi-body system, or a stiff mass-

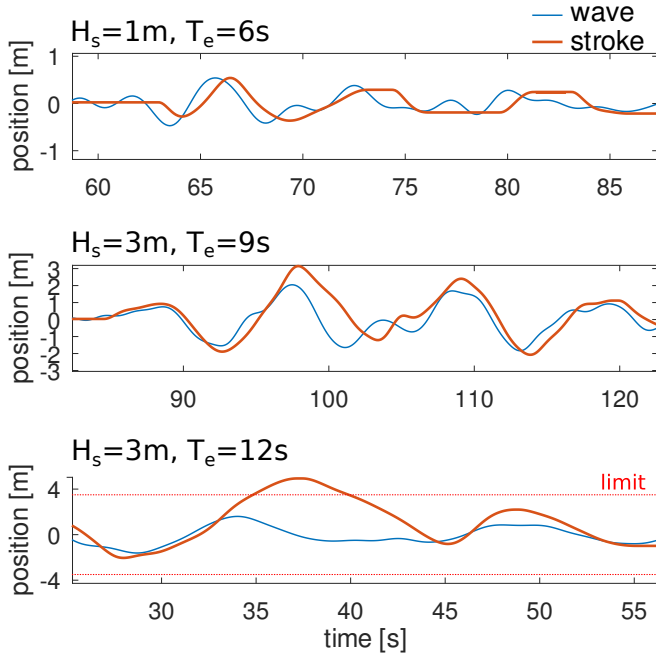


Fig. 3. Time domain characteristics of different sea states: Top: Low energy sea state, dominated by stick-slip friction. Middle: Medium energy sea state: No significant stick-slip effect, far away from the stroke constraints. Bottom: High energy sea state: Stroke constraints are exceeded.

spring-damper system, are high. The mooring line is, as a consequence, modelled as a stiff connection, with a universal joint at the seabed anchor point.

For a graphical overview of the effects included see also Figure 1.

### B. Constraints

For a realistic device, the controller must ensure that it operates within the WEC design constraints, to prolong the device lifetime. For the COERbuoy1 device, the stroke length is limited to  $\pm 3.5$  m with respect to the equilibrium position; since the generator can get saturated, the maximum generator damping can be derived from the generator equation. The stroke limit is not modelled as a physical end-stop, but violations of the stroke length are penalised by a lower benchmark score. See Section IV for details.

### C. Characteristics

Based on the features presented in Subsections II-A and II-B, three different operational characteristics, due mainly to the prevailing sea state, can be distinguished (see also Figure 3):

- In low energy sea states, friction (especially the stick-slip effect) is dominant. The uncontrolled WEC motion is difficult to predict.
- For medium energy sea states, the stick-slip effect is less important, and the stroke motion does not reach the limits.
- In high energy sea states, the stick-slip effect is negligible; however, the stroke length may easily exceed the safe stroke length and must be limited.

TABLE II  
SENSOR DATA AND MANIPULATED VARIABLES

Variable	Quantity	Units
Sensor data		
$\zeta$	Stroke length	m
$\alpha$	Pitch angle	rad
$\dot{\zeta}$	Stroke velocity	m/s
$\dot{\alpha}$	Pitch angular velocity	rad/s
$F_{mo}$	Force on the mooring	N
Manipulated variables		
$F_{gen}$	Generator force	N
$F_{br}$	Braking force	N

### D. Manipulated variables and sensor measurements

The COERbuoy1 simulation provides a controller interface where a set of measured data is made available. In return it takes the values for the manipulated variables. See Table II for the exchanged data. The measured data consists of the stroke length, the pitch angle of the WEC, both relative to the equilibrium position (see Figure 5), and the force along the mooring line. Neither the wave elevation or excitation force is directly measured, and must, if needed, be estimated from the measured data. All sensor data in the model are noise-free and unbiased. The controller can set the generator force and the braking force, so that the WEC is controlled in one of three possible ways: (i) By setting the generator resisting force the WEC can be controlled passively, applying a generator force opposing the direction of travel (passive control) or (ii) actively, by putting power into the generator (active control) at various intervals, causing a force in the direction of travel. It should be noted that the generator has equal internal losses in both power flow directions, thus bidirectional power must be used carefully. (iii) The third option is dissipative braking, where the force is only limited by the maximal braking power  $P_{br}^{max}$ . There are no costs for applying the brake, the energy however, unlike the PTO-force, is transformed to heat, and not absorbed.

## III. MATHEMATICAL DESCRIPTION OF THE MODEL

This Section gives a brief overview of the mathematical modelling of the device. More details and the source code are available at [14].

### A. Overview of forces

The COERbuoy1 platform simulates a buoy in two degrees-of-freedom (DOF) (heave and surge), in the time-domain. The motion of the system, in the time-domain, is expressed as:

$$M\ddot{\vec{x}}_{fl} = \vec{F}_{ex} + \vec{F}_{rad} + \vec{F}_{h,st} + \vec{F}_{drag} + \vec{F}_{PTO} + \vec{F}_m + \vec{F}_{sp} + \vec{F}_t + \vec{F}_g + \vec{F}_{br} \quad (1)$$

where  $\vec{F}_{ex}$  is the excitation force,  $\vec{F}_b$ , the buoyancy force,  $\vec{F}_{rad}$  the radiation force,  $\vec{F}_{PTO}$  is the PTO force

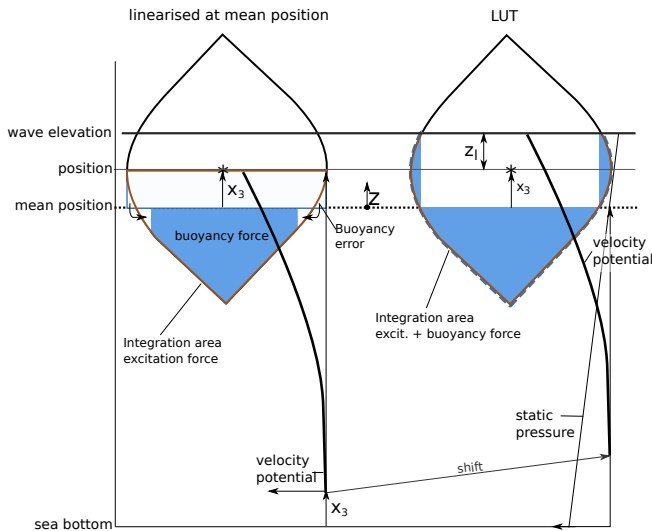


Fig. 4. Calculation of the excitation force and buoyancy force for the pure linear and body-exact case: The outline of the wetted surface over which the excitation force is integrated, is drawn in brown, while the cross-sectional area of the buoyancy volume is drawn in light blue. It can be seen, that the base for all hydrodynamic calculations of the purely linear approach is the mean body position. The wave elevation is neglected. Due to the convex-shape, the buoyancy force is underestimated, visualized with the exclusion of the triangular shape in the buoyancy area. In contrast, the body-exact approach considers the wave elevation and calculates the forces based on the actual wetted surface. Therefore, it must shift the velocity potential. For further information on the buoyancy force calculation, the interested reader is referred to [15].

modulated by the controller,  $\vec{F}_{drag}$  the viscous drag force,  $\vec{F}_m$  is the machinery friction force,  $\vec{F}_{sp}$  the force of the negative spring,  $\vec{F}_g$  the force due to gravity,  $\vec{F}_{br}$  the force applied by the brake, and  $\vec{F}_t$  the pre-tension force between machinery and buoy.  $M$  is a matrix containing the mass Matrix  $M^m$  and the added mass matrix  $M^{add}$ :  $M = M^m + M^{add}$ . The position vector, in global coordinates, for surge ( $x_1$ ) and heave ( $x_3$ ) is  $\vec{x}_p = [x_1 \ x_3]^T$ . The global coordinates are transferred into body coordinates described in polar coordinates by the stroke length  $\zeta$  and the pitch angle  $\alpha$  of the mooring line as shown in Figure 5:

$$\vec{\zeta} = \begin{bmatrix} \zeta \\ \alpha \end{bmatrix} = \begin{bmatrix} \|\vec{x}_p\| \\ \angle(x_p + l_m) \end{bmatrix}, \quad (2)$$

with  $l_m$  being the mooring length. The forces are described in detail in Subsections III-B and III-C.

### B. Hydrodynamic forces

Hydrodynamic modelling of WECs is a challenge, since high-fidelity approaches, like computational fluid dynamics (CFD), are computationally expensive. To assess the performance of WECs, it has become common practice to use linear hydrodynamic theory, using boundary element methods (BEMs) to solve the equations. While orders of magnitude quicker than CFD, BEMs are computationally too demanding to be solved in real-time on regular desktop computers. Therefore, linearisation of the hydrodynamic WEC parameters, using pre-calculated data at the mean or equilibrium position of the WEC, are widely used. For large relative movements of the WEC, with respect to

the mean position, commonly seen for WECs using energy-maximising controllers, this approach has been shown to be inaccurate [4]. This subsection gives a brief overview of linear hydrodynamics and body-exact calculations, followed by the calculation of the resulting hydrodynamic parameters.

a) *Linear hydrodynamics*: Airy wave theory is used to describe the waves, providing a linear mathematical description for non-steep, non-breaking waves in an inviscid, incompressible and irrotational fluid. Consequently, waves can be described in an analytical way, with the central quantity being the velocity potential,  $\phi$ , defined through:

$$\vec{v} = \left[ \frac{\partial \phi}{\partial x}, \frac{\partial \phi}{\partial y}, \frac{\partial \phi}{\partial z} \right]^T = \nabla \phi, \quad (3)$$

with  $\vec{v}$  being the fluid velocity vector,  $x, y$  the horizontal Cartesian coordinates and  $z$  the vertical coordinate with  $z = 0$  commonly defined at the mean water level. Boundary conditions for the seabed, the free-surface elevation and the body boundary are needed to solve the problem, see [16] for a detailed description. Linear theory permits the representation of panchromatic waves as a (polychromatic) sum of monochromatic waves, each with wave elevation  $\eta_i$ , specified by its amplitude  $a_i$ , wave frequency  $\omega_i$ , wave number  $k_i$  and phase offset  $\xi_i$ :

$$\eta_i(x, t) = a_i \cos(\omega_i t - k_i x + \xi_i) \quad (4)$$

$$\eta(x, t) = \sum_i \eta_i(x, t). \quad (5)$$

b) *Body-exact forces*: Linear hydrodynamics assumes a small wave-body movement, so that the hydrodynamic parameters are time/position independent. With increasing wave height and relative wave-body motion, these assumptions do not hold, leading to the necessary specification of body-exact forces. While not strictly accurate from a mathematical standpoint, the body-exact assumption has shown superior behaviour over purely linear models [17]–[20]. Two ways of correcting linear hydrodynamic theory with body-exact forces, from the literature include: (i) Using only body-exact Froude-Krylov forces [15] in combination with pre-calculated (using BEM) radiation and diffraction coefficients for the mean position. (ii) Using pre-calculated hydrodynamic parameters for different body positions stored in a look-up-table (LUT) that is used during run-time [17], [21]. As only the LUT method provides all hydrodynamic parameters in a body-exact representation, this approach is used for the COERbuoy1 platform.

c) *Hydrodynamic calculations*: Using linear hydrodynamic theory, wave-body interaction can be described as the superposition of three subproblems, dealing with forces due to: (1) the undisturbed incoming wave, (2) the scattered wave field by the non-moving buoy, and (3) the radiated wave caused by the buoy's movement [16]. When neglecting the motion of the body, the integration of the velocity potential, for the undisturbed incoming (1) and scattered wave

(2)  $(\phi_{ex})$  over the wetted surface  $S_w$ , results in the excitation force:

$$F_{e,j} = \rho g \iint_{S_w} \phi_{ex} n_j dS, \quad (6)$$

with  $g$  being the acceleration due to gravity,  $\rho$  being the density of water,  $n$  being the unit normal vector and  $j$  the specific degree of freedom ( $j=1$  is surge;  $j=3$  is heave). Similarly, the radiation force (3), the integration of the velocity potential for the radiated wave,  $\phi_R$ , related to the current and past motion of the body, over the wetted surface, is:

$$F_{r,j} = \rho g \iint_{S_w} \phi_R n_j dS. \quad (7)$$

The hydrostatic force, here called the buoyancy force, is the force related to the static hydrodynamic pressure  $p_{st} = g\rho z$ :

$$F_{b,z} = \iint_{S_w} p_{st} n_z dS. \quad (8)$$

Both are defined for  $z < 0$ , that is the volume below the mean surface level. Unlike pure linear hydrodynamic theory, body-exact methods consider the current wave height  $\eta$ , instead of assuming an infinitesimal wave height. Consequently the velocity potential must be adapted to the currently-exact free-surface elevation, commonly done using Wheeler stretching [22]. The hydrodynamic coefficients in the LUT are pre-calculated at the mean water level, thus taking the surface elevation into account, this corresponds to a shift of the velocity potential to the free surface  $z_0 \rightarrow \eta$ , rather than being Wheeler stretched. However, the differences should be small. The instantaneous submergence level, for which the hydrodynamic parameters are requested from the LUT is  $z_l = \eta - x_3$ . See Figure 4 for a sketch of the hydrodynamic calculations for pure linear theory and the body-exact LUT approach used here.

*d) Instantaneous linearisation:* Solving (6) and (7) is computationally demanding. Using linearisation at the body-position  $\vec{x}_p$ , the resulting forces can, in the frequency domain, be obtained by multiplications: (a) The excitation force, the combination of the forces caused by the incoming and scattered waves, both related to the incoming wave amplitude  $\boldsymbol{\eta}$  (here **bold** symbols define vectors in frequency domain), is:

$$\mathbf{F}_{e,j} = \mathbf{h}_j(\vec{x}_{p,j})\boldsymbol{\eta}, \quad (9)$$

with  $\mathbf{h}(\vec{x})$  being the buoy position dependent excitation force coefficients. (b)  $\vec{F}_{rad}$ , the force caused by the radiated wave, depends on the current and previous values of the buoy velocity. For small wave-body motion, the hydrodynamic coefficients can be assumed constant and, therefore, the radiation force calculated in the frequency domain is, similarly to the excitation force, a multiplication between the radiation force coefficients  $\mathbf{R}$  and the Fourier transform of the buoy velocity. In contrast, the body-exact radiation forces, assuming non-constant hydrodynamic parameters, need to be calculated in the time domain. In the following, Cummins convolution term for the radiation force [23] is modified: The radiation coefficients in the frequency

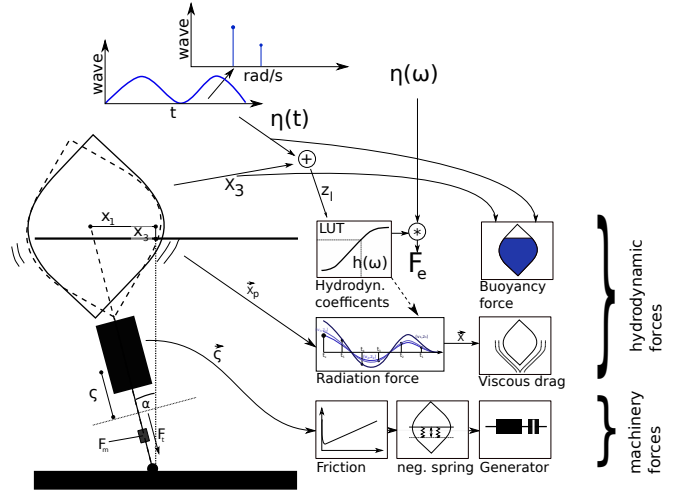


Fig. 5. Schematic of the COERbuoy1 model.

domain are scaled by the instantaneous excitation coefficients in relation to the excitation coefficients at the time of the creation of the corresponding radiated wave. Then, the modified radiation coefficients are transformed into the time domain, giving:

$$\vec{F}_{r,j}(t_x) = \sum_{k=1}^{DOF} \int_0^{t_x} \left( \int_{\omega} \mathbf{h}_j(\vec{x}_{p,j}(t_x)) \mathbf{R}_{j,k}(\vec{x}_{p,j}(\tau)) / \mathbf{h}(\vec{x}_{p,j}(\tau)) \cos(\omega\tau) d\omega \right) \delta(\tau) \dot{x}_{w,k}(\tau) d\tau, \quad (10)$$

with  $\vec{x}(\tau)$  being the buoy position vector at time  $\tau$ ,  $\dot{x}_{w,k}$  the relative velocity between wave and buoy in degree of freedom  $k$ , where  $\delta$  is the Dirac impulse.

The hydrodynamic parameters  $\mathbf{h}$  and  $\mathbf{R}$  are calculated for different buoy positions, using the BEM solver NEMOH [24], assuming an infinitely wide and deep ocean. The LUT performs linear interpolation between the values obtained from NEMOH. The buoyancy force is obtained by integrating the static pressure over the wetted surface of the buoy, as described in [15].

*e) Viscous damping:* While linear hydrodynamic theory includes only linear effects, it has been shown that, due to the large motion of WECs, viscous damping becomes a relevant nonlinear force. It is considered on the basis of  $A_{c,j}$ , the projected area of the submerged volume of the buoy in direction  $j$ :

$$\vec{F}_{drag,j} = 0.5c_{D,j} \dot{x}_j |\dot{x}_j| A_{c,j} \rho. \quad (11)$$

### C. Machinery forces

*a) Stribeck friction:* The machinery losses include the losses due to friction, and generator losses. The Stribeck curve, including static friction  $F_{fr,s}$ , dynamic friction  $F_{fr,k}$ , and a friction damping term  $\gamma_f$ , is implemented as a non-continuous force:

$$\ddot{\zeta} = 0, \quad \text{if } \dot{\zeta} = 0 \wedge |M\ddot{x}\vec{n}_\zeta| \leq F_{fr,s} \quad (12)$$

$$F_m = F_{fr,k} + \gamma_f \dot{\zeta}, \quad \text{otherwise.} \quad (13)$$

b) *PTO*: A gearbox with gear ratio  $n_{gb}$  transforms the translatory stroke speed  $\dot{\zeta}$  into the angular generator speed  $\omega_g$ . Assuming that reactive power flow is set to zero by the generator's internal controller, the generator voltages, in the  $p - q$  frame, becomes:

$$U_d = -R_c I_d - c_{Ld} \dot{I}_d + \dot{\zeta} I_q c_{Lq} \quad (14)$$

$$U_q = R_c I_q - c_{Lq} \dot{I}_q - \dot{\zeta} (I_d c_{Ld} - c_\lambda), \quad (15)$$

where  $R_c$  is the inner electrical resistance of the PTO,  $c_{Ld}$  and  $c_{Lq}$  the inductance related coefficients (including the gearbox ratio) for the  $p$  and  $q$  currents, and  $c_\lambda$  a constant related to the flux linkage. A perfect motor controller is assumed, so that  $I_d = 0$  at all times, and thus  $U_d = \dot{\zeta} I_q c_{Lq}$ . The voltage source  $U_q$  is described as a resistance  $R_g$ , which can be positive (motor mode), or negative (generator mode) i.e.  $U_q = R_g I_q$  giving:

$$0 = c_{Lq} \dot{I}_q + (R_c - R_g) I_q - \dot{\zeta} c_\lambda, \quad (16)$$

with  $\dot{I}_q = \dot{\zeta} I_q$ . From (16), the PTO-force becomes:

$$F_{pto} = \frac{(\dot{\zeta} c_\lambda)^2}{(c_{Lq} \dot{\zeta})^2 + (R_c - R_g)^2} \frac{(R_c - R_g)}{\dot{\zeta}}. \quad (17)$$

From (17), the generator resistance  $R_g$  is obtained to calculate  $I_q$ , and finally the absorbed power is:

$$P_{abs} = R_g I_q^2 = R_g 2\pi / w_p (n_g \dot{\zeta})^2 = c_R \dot{\zeta}^2, \quad (18)$$

with  $w_p$  being the pole pair width. To limit the maximum generator damping, magnetic saturation is modelled by introducing the saturation factor  $\gamma_s$ , setting the momentary current  $I_q$  in relation to the current  $I_s$  where saturation starts:

$$\gamma_s = \frac{I_s}{I_q}. \quad (19)$$

Then, the new inductance factor  $c_{Lqs}$  is calculated, it replacing  $c_{Lq}$  in (15):

$$c_{Lqs} = c_{Lq} (1 + D), \quad (20)$$

with

$$D = \begin{cases} 1 & I_q < I_s \\ 2/\pi \left( \arctan \left( \frac{\gamma_s}{\sqrt{1-\gamma_s^2}} \right) + \gamma_s \sqrt{1-\gamma_s^2} \right) & \text{otherwise} \end{cases} \quad (21)$$

This method was evaluated with a full-scale wave energy generator in [25].

When exceeding the stroke limits  $\pm s_{lim}$ , the generated power cannot be utilised and is therefore not considered in the calculated overall energy output; reactive power put into the generator, however, is always subtracted from the total absorbed energy.

c) *Pre-tension*: The pre-tension force  $\vec{F}_t$  allows the buoy's gravity force, and therefore its mass, to be lower than the buoyancy force at the equilibrium position, and is calculated as the mismatch between the gravity and buoyancy forces at the equilibrium position:

$$F_{t,j} = V_0 \rho g (1 - c_{m,f}), \quad (22)$$

where  $V_0$  is the submerged volume at the equilibrium position, and  $c_{m,f} \in (0, 1]$  is the ratio  $m/(V_0 \rho)$ .

TABLE III  
TABLE OF THE SELECTED PARAMETERS OF THE  
COERBUOY1 MODEL

Symbol	Quantity	Value
$c_s$	negative spring stiffness	0.3 GN/m
$l_s$	compressed neg. spring length	1.5 m
$c_{mf}$	relative mass WEC	1/4 <sup>a</sup>

<sup>a</sup> The mass is denoted relative to the buoyancy force at equilibrium position. The remaining buoyancy force is the pre-tension of the mooring.

d) *Braking force*: The braking force  $F_{br}$  opposes the direction of travel and can be set to an arbitrary value within the power limit  $P_{br}^{max}$ :

$$F_{br} \dot{\zeta} < P_{br}^{max}. \quad (23)$$

#### IV. EVALUATION AND SCORING

A WEC controller should maximise power generation within the constraints. Equally important in certain scenarios, but not considered in this benchmark, is a smooth power output.

As sea states at one location can vary widely over a year, these control demands must be achieved in sea states differing in terms of characteristic wave height, wavelength and spectral shape. Furthermore, mathematical models, as simplified representations of reality, cannot be accurate in all aspects, thus a real WEC controller should be robust to modelling errors and ideally adapt to systematic biases in the real system. The following Subsection IV-A will present the sea states used in the benchmark, and Subsection IV-B presents the criteria used to evaluate the controller performance, and the process to calculate the final score. It should be kept in mind, that a benchmark score can only provide a rough assessment, it is not a panacea and cannot replace the detailed evaluation that must be part of a controller design. The COERbuoy1 platform aims to support this process by providing all necessary information.

##### A. Benchmark stages

As presented in Section I, WEC controllers must perform well over a wide range of scenarios. Therefore, a staged evaluation process is used, consisting of three categories, each of which uses four sea states:

- (I) The first stage comprises regular (monochromatic) waves, then
- (II) the second stage evaluates the controller's ability to capture power from wide-band spectra, using irregular (panchromatic) sea states, based on the Bretschneider spectrum.
- (III) The third stage uses the irregular sea states from (II), but changes the hydrodynamic parameters, to test, depending on the controller design, either the controller's ability to adapt to a systematic bias or its robustness to modelling errors.

Regular waves and Bretschneider spectra sea states are at the extremities of ocean wave spectra bandwidth. For swell seas, regular waves results may be more

representative than the wide bandwidth Bretschneider spectra. Furthermore, performance in narrow bandwidth regular waves or wide bandwidth Bretschneider sea states are different challenges, from a control perspective. When comparing the results of stages (I) and (II), valuable insights in the controller's ability to optimize for different frequencies and to forecast the waves can be obtained.

To increase readability, the regular waves are shortened to the form  $(T_w, H_{RMS})$ , where the first value indicates the wave period ( $T_w$ ) in seconds and the second number corresponds to the root-mean square wave height ( $H_{RMS}$ ) in meters. Similarly, the irregular sea states are shortened to the form  $\{T_e, H_s\}$ , where the first number corresponds to the energy period ( $T_e$ ) in seconds, and the second number indicates the significant wave height ( $H_s$ ) in meters.

a) *Regular wave stage*: Four regular waves are used to evaluate the narrow-band absorption characteristics, corresponding to the three operational characteristics from Figure 3: One low energy sea state (6, 1), two medium energy sea states, only differing in the wave period (9, 1.5 & 9, 3), and one high energy sea state (12, 3), form the regular test.

b) *Irregular sea states stage*: The irregular sea states, based on the Bretschneider spectrum, are determined with parameters  $\{6, 1\}$ ,  $\{9, 1.5\}$ ,  $\{9, 3\}$  and  $\{12, 3\}$ . A deterministic amplitude scheme, using pseudo-random phases, is used to create the time-series, as this gives accurate estimates of the long-term wave characteristics for shorter simulation periods, compared to a random amplitude scheme [26]. The regular, and its corresponding irregular sea state, transport the same amount of energy, where the correspondence is  $(T_w, H_{RMS}) \equiv \{T_e, H_s\}$ . The Bretschneider spectrum, describing a not fully developed sea, is chosen, as it is a wide band spectrum, compared to the JONSWAP spectrum, and therefore creates a contrast to the regular wave benchmark stage.

c) *Systematic modelling error test*: Inspired by [27], the sensitivity of the controller to modelling errors is tested by repeating the irregular sea state but changing the parameters for each sea state with pseudo-random values. These changed aim to represent arbitrary, systematic modelling errors. This means that the controller has to estimate and adapt to this error, or have some feature making it robust enough to handle these changes. The controller should not know these values *a priori*. Each sea state in stage three is run four times, with different sets of parameters. The mean score of all runs is used as the score for this sea state. The pseudo-random values are hard-coded, thus the same combination of parameter, sea state and run will appear at every benchmark test. To prevent control designers from cheating, the order in which the tests are run can vary.

## B. Scoring

The controller is assessed by its generated electric energy and how well it adheres to the constraints, resulting in a power score  $S_p$  and a constraint score  $S_c$  which, multiplied, give the benchmark score  $S_S$ .

a) *Power score*: Each benchmark stage, as indicated in Subsection IV-A, consists of four sea states with increasing maximal unconstrained converted power  $P_{max}$ , as can be seen in Table IV, where the maximum unconstrained absorbable power [16] is:

$$\begin{aligned} P_{max} &= 6\rho g^3 / (128\pi^3) T_e^3 H_s^2 \\ &= 6\rho g^3 / (128\pi^3) T_w^3 H_{rms}^2 \end{aligned} \quad (24)$$

It should be noted that the maximum power cannot be absorbed for all sea states, due to the stroke limit  $s_{lim} = \pm 3.5$  m. For the power score ( $S_p$ ), a convenient and easy to interpret number is needed, therefore  $S_p$  is calculated as the ratio of the absorbed power  $P_{abs}$  and the absorbed power by a constrained complex-conjugate controller  $P_{ccc}$  as presented in [28], assuming an ideal, linear, heave only, model:

$$S_p = \max(P_{gen}/P_{ccc}, 0). \quad (25)$$

Negative values for  $S_p$ , when more electrical power is, on average, put into the PTO than generated, corresponding to a very poor performing controller, are set to zero.

$P_{ccc}$  is calculated as:

$$P_{ccc} = \begin{cases} \hat{F}_e(T_w)^2 / (8R(T_w)) & , \text{ if } \max(\zeta) < s_{lim} \\ 0.5u^2(\hat{F}_e(T_w)/u - R(T_w)) & , \text{ otherwise} \end{cases} \quad (26)$$

with  $u = s_{lim}2\pi/T_w$  and  $\hat{F}_e = 0.5H_{rms}\sqrt{2}h(T_w)$ . It should be noted that  $S_p < 1$ , due to the nonlinear viscous drag and losses in the machinery.

b) *Constraint score*: The constraints score  $S_c$  is the duration  $t_c$ , in seconds, the limits are exceeded, in relation to the duration of sea state  $t_d$ :

$$S_c = t_c/t_d. \quad (27)$$

c) *Total score*: The sum  $S_{s,ss,sg}$  for each sea state  $ss$  at stage  $sg$  is the product of the power score  $S_{p,ss,sg}$  and the constraint score  $S_{c,ss,sg}$ :

$$S_{s,ss,sg} = S_{p,ss,sg}S_{c,ss,sg} \quad (28)$$

The score for each stage is the mean of all sea state scores:

$$S_{s,sg} = \sum_{ss=1}^4 S_{s,ss,sg}. \quad (29)$$

Subsequently, the final score is the mean of the scores for all stages:

$$S_S = \sum_{sg=1}^3 S_{s,sg}. \quad (30)$$

Additionally, information such as the 95% quantile for the machinery excursion, velocity and force, are calculated and presented in the benchmark results, but are not part of the scoring. Even so, they might be important data for the evaluation of a controller. An early draft of the certificate generated by the COERbuoy1 benchmark can be seen in Figure 6.

TABLE IV  
TABLE OF SEA STATES USED IN THE BENCHMARK

$H_{rms}/H_s$ [m]	$T_w/T_e$ [s]	$P_{max}$ [kW]	$P_{ccc}$ [kW]
1	6	308.8	102.6
1.5	9	2344.6	426.9
3	9	9378.4	938
3	12	22230.3	826.3

$H_{rms}$  and  $T_p$  apply for a regular wave, and  $H_s$  and  $T_e$  apply for an irregular sea state.

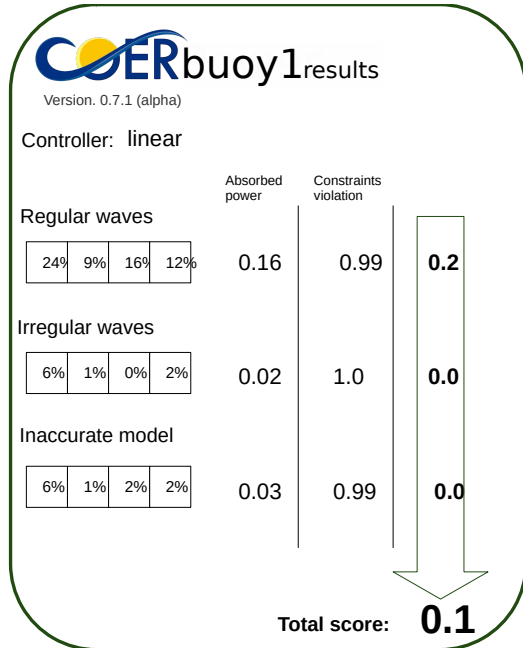


Fig. 6. Draft of the benchmark certificate.

## V. EXAMPLE

For illustration, the presented model and benchmark system is now tested with a simple constant damping PTO:  $F_{pto} = \gamma \dot{\zeta}$ , with  $\gamma = 100$  kNs/m.. The damping is the optimal damping, obtained with a damping sweep, for the regular wave with  $H_{RMS} = 1$  m and  $T_w = 4.5$  s, a wave period close to the resonance period of the device.

a) *Constant damping*: While being the simplest form of a PTO, a generator applying a constant damping (within the limits of saturation) is widely used in full-scale WECs [29], [30], as it corresponds to a constant load for electric generators. With its simplicity, it might be seen as the lower bound of achievable performance. However, the resulting unidirectional power flow guarantees that more power is absorbed than is put into the system; a feature an active (bidirectional power flow) control design cannot guarantee.

b) *Results & Discussion*: The scoring of the constant damping control can be seen in Table V, and the time series of selected sea states of the test run in Figure 3. The highest score is obtained for the 6 s period wave, the period closest to the natural frequency of the WEC. For the 9 s and 12 s wave periods, linear damping performs much worse than for the 6 s wave period sea states. In regular waves, the stick-slip effect plays a minor role compared to the irregular cases, where small waves alternate with large waves. This results

in a significantly lower power score for the irregular waves (about 1/10th) than for the regular waves. The constant damping does not actively exaggerate the motion, yet the constraints are violated for sea state 4 in stage (I) and (III), however, the constraint score  $S_c$  is only lowered by about 3% having no significant influence on the results.

It should be noted that the COERbuoy1 platform used for evaluation is still in an early beta phase; some refinement of parametric settings, etc. may occur in response to user feedback.

## VI. TECHNICAL DETAILS

The source code of the COERbuoy1 platform is publicly available at [14] and is designed to run out-of-the box on all major computer platforms. This section briefly outlines the structure of the platform and the interface provided.

The COERbuoy1 platform is written in Python with an optional user interface, developed in HTML/JavaScript, running as a web server, enabling the software to run under any platform with Python support. The command-line interface can be accessed from the Python interpreter, but also from MATLAB and Octave (via Pythonic), allowing for easy integration of COERbuoy1 in user programs.

The code structure can be seen in Figure 7: The COERbuoy1 platform offers a user interface (GUI/CLI) and an interface for the control algorithm. The control interface uses a TCP/IP connection, since TCP/IP libraries are available for almost all programming languages; thus the controller can be written independently of the COERbuoy1 platform. Furthermore, the separation of controller and model eases the integration of the controller with physical WEC models and WECs operating in the ocean.

The computational speed of the COERbuoy1 platform is similar to time domain WEC models with linear hydrodynamics. On most computers the simulated time will be close to the elapsed wall-clock time.

## VII. CONCLUSIONS & OUTLOOK

A benchmarking tool, named COERbuoy1, for the assessment of the performance of energy maximising WEC controllers under realistic conditions is presented, combining a wave-to-wire model inspired by an industrial WEC design, with an evaluation system for WEC controllers. Unlike most models used in the WEC community, the COERbuoy1 platform is open source and aims for easy integration in existing workflows, by separating the controller from the model.

The benchmark process, made up of three categories, has been tested for a simple constant damping PTO design, which can be seen as a lower bound for all further controller tests. The constant damping performed well for sea states with a short wave period, close to the natural frequency of the device. For the more powerful, long period, sea states, however, the scores were low. Despite a significant constraint violation, the constraint violation penalty was only marginal.

The software is currently in beta phase and will be released in a final version in October 2021.

TABLE V  
BENCHMARKING RESULTS FOR CONSTANT DAMPING OF 100 kNs/M POWER-TAKE-OFF

	sea state 1			sea state 2			sea state 3			sea state 4			total scores			
	$S_p$	$S_c$	$S_s$	$S_p$	$S_c$	$S_s$										
regular	0.24	1	0.24	0.1	1	0.1	0.16	1	0.16	0.13	0.97	0.13	0.16	0.99	0.16	
irregular	0.06	1	0.06	0.02	1	0.02	0.02	1	0.02	0.02	1	0.02	0.03	1	0.03	
modelling errors	0.06	1	0.06	0.02	1	0.02	0.02	1	0.02	0.03	0.974	0.03	0.03	0.99	0.03	
													Total:	0.07	0.99	<u>0.07</u>

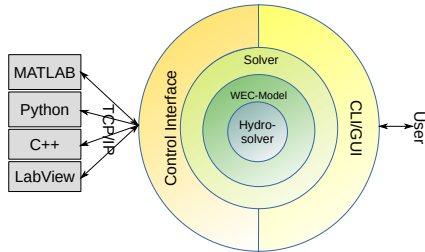


Fig. 7. Structure of the COERbuoy1 platform: The hydrodynamics, the model and the solver are encapsulated; a (graphical) user interface and the control interface allow for easy communication with the model.

#### ACKNOWLEDGEMENTS

The authors would like to thank Giuseppe Giorgi from Politecnico di Torino, for his help in understanding hydrodynamics, Hafiz Ahsan Said, for his help with the generator model, and Carrie Anne Barry, both from COER. This research was part-funded by Science Foundation Ireland (SFI) through MaREI, the SFI Research Centre for Energy, Climate, and Marine [Grant No: 12/RC/2302\_P2], with supporting funding obtained from CorPower Ocean AB.

#### REFERENCES

- [1] H. Titah-Benbouzid and M. Benbouzid, "An up-to-date technologies review and evaluation of wave energy converters," *International Review of Electrical Engineering (IREE)*, vol. 10, 02 2015.
- [2] B. Drew, A. R. Plummer, and M. N. Sahinkaya, "A review of wave energy converter technology," *Proceedings of the Institution of Mechanical Engineers, Part A: Journal of Power and Energy*, vol. 223, no. 8, pp. 887–902, 2009.
- [3] L. Wang, J. Engström, M. Göteman, and J. Isberg, "Constrained optimal control of a point absorber wave energy converter with linear generator," *Journal of Renewable and Sustainable Energy*, vol. 7, no. 4, p. 043127, 2015.
- [4] C. Windt, N. Faedo, M. Penalba, F. Dias, and J. V. Ringwood, "Reactive control of wave energy devices – the modelling paradox," *Applied Ocean Research*, vol. 109, p. 102574, 2021.
- [5] J. Todalshaug, J. Falnes, and T. Moan, "A comparison of selected strategies for adaptive control of wave energy converters," *Journal of Offshore Mechanics and Arctic Engineering*, vol. 133, 03 2011.
- [6] P. B. Garcia-Rosa and J. V. Ringwood, "On the sensitivity of optimal wave energy device geometry to the energy maximizing control system," *IEEE Transactions on Sustainable Energy*, vol. 7, no. 1, pp. 419–426, 2016.
- [7] D. García Violini, N. Faedo, F. Jaramillo-Lopez, and J. Ringwood, "Simple controllers for wave energy devices compared," *Journal of Marine Science and Engineering*, vol. 8, p. 793, 10 2020.
- [8] N. Faedo, D. García Violini, Y. Peña Sanchez, and J. Ringwood, "Optimisation-vs. non-optimisation-based energy-maximising control for wave energy converters: A case study," 05 2020.
- [9] N. Faedo, S. Olaya, and J. V. Ringwood, "Optimal control, mpc and mpc-like algorithms for wave energy systems: An overview," *IFAC Journal of Systems and Control*, vol. 1, pp. 37–56, 2017.
- [10] J. Ringwood, F. Ferri, K. M. Ruehl, Y.-H. Yu, R. G. Coe, G. Baccelli, J. Weber, and M. Kramer, "A competition for wec control systems," in *12th European Wave and Tidal Energy Conference, Cork, Ireland*, 2017.

- [11] M. Penalba and J. V. Ringwood, "A review of wave-to-wire models for wave energy converters," *Energies*, vol. 9, no. 7, 2016.
- [12] A. Têtu, *Power Take-Off Systems for WECs*. Cham: Springer International Publishing, 2017, pp. 203–220.
- [13] R. Ahamed, K. McKee, and I. Howard, "Advancements of wave energy converters based on power take off (pto) systems: A review," *Ocean Engineering*, vol. 204, p. 107248, 2020.
- [14] S. Thomas, "The COERbuoy1 platform." [Online]. Available: <http://coerbuoy.maynoothuniversity.ie>
- [15] G. Giorgi and J. V. Ringwood, "Analytical representation of nonlinear froude-krylov forces for 3-dof point absorbing wave energy devices," *Ocean Engineering*, vol. 164, pp. 749 – 759, 2018.
- [16] J. Falnes, *Ocean Waves and Oscillating Systems: Linear Interactions Including Wave-Energy Extraction*. Cambridge: Cambridge University Press, 2002.
- [17] S. Rajendran, N. Fonseca, and C. Guedes Soares, "Prediction of vertical responses of a container ship in abnormal waves," *Ocean Engineering*, vol. 119, pp. 165–180, 2016.
- [18] A. Merigaud, J.-C. Gilloteaux, and J. V. Ringwood, "A Non-linear Extension for Linear Boundary Element Methods in Wave Energy Device Modelling," in *Symposium on Offshore and Ship Hydrodynamics*, ser. International Conference on Offshore Mechanics and Arctic Engineering, vol. 4: Offshore Geotechnics; Ronald W. Yeung Honoring, 07 2012, pp. 615–621.
- [19] A. Babarit, H. Mouslim, A. Clément, and P. Laporte-Weywada, "On the Numerical Modelling of the Non Linear Behaviour of a Wave Energy Converter," in *Proceedings of the ASME 2009 28th International Conference on Ocean, Offshore and Arctic Engineering*, vol. 4, 05 2009, pp. 1045–1053.
- [20] B. Schubert, W. Robertson, B. Cazzolato, and M. Ghayesh, "Linear and nonlinear hydrodynamic models for dynamics of a submerged point absorber wave energy converter," *Ocean Engineering*, vol. 197, p. 106828, 02 2020.
- [21] B. Schubert, F. Meng, N. Sergiienko, W. Robertson, B. Cazzolato, M. Ghayesh, A. Rafiee, B. Ding, and M. Arjomandi, "Pseudo-nonlinear hydrodynamic coefficients for modelling point absorber wave energy converters," in *The 4th Asian Wave and Tidal Energy Conference, Taiwan*, 09 2018.
- [22] J. Wheeler, "Method for Calculating Forces Produced by Irregular Waves," *Journal of Petroleum Technology*, vol. 22, no. 03, pp. 359–367, 03 1970.
- [23] W. Cummins, *The Impulse Response Function and Ship Motions*, ser. Report (David W. Taylor Model Basin). Navy Department, David Taylor Model Basin, 1962.
- [24] A. Babarit and G. Delhommeau, "Theoretical and numerical aspects of the open source BEM solver NEMOH," in *11th European Wave and Tidal Energy Conference (EWTEC2015)*, Nantes, France, Sep. 2015.
- [25] R. Krishna, O. Svensson, M. Rahm, S. K. Kottayil, R. Waters, and M. Leijon, "Analysis of linear wave power generator model with real sea experimental results," *IET Renewable Power Generation*, vol. 7, no. 5, pp. 574–581, 2013.
- [26] A. Mérigaud and J. V. Ringwood, "Free-surface time-series generation for wave energy applications," *IEEE Journal of Oceanic Engineering*, vol. 43, no. 1, pp. 19–35, 2018.
- [27] Y. Zhang and G. Li, "Non-causal linear optimal control of wave energy converters with enhanced robustness by sliding mode control," *IEEE Transactions on Sustainable Energy*, vol. 11, no. 4, pp. 2201–2209, 2020.
- [28] D. Evans, "Maximum wave-power absorption under motion constraints," *Applied Ocean Research*, vol. 3, no. 4, pp. 200–203, 1981.
- [29] E. Lejerskog, C. Boström, L. Hai, R. Waters, and M. Leijon, "Experimental results on power absorption from a wave energy converter at the lysekil wave energy research site," *Renewable Energy*, vol. 77, pp. 9–14, 2015.
- [30] M. Prado and H. Polinder, "Direct drive in wave energy conversion — AWS full scale prototype case study," in *2011 IEEE Power and Energy Society General Meeting*, 2011, pp. 1–7.